HHS Public Access

Author manuscript

*J Neurochem*. Author manuscript; available in PMC 2016 June 01.

Published in final edited form as:

*J Neurochem*. 2015 June ; 133(5): 668–683. doi:10.1111/jnc.13040.

# Molecular mechanisms of non-transferrin-bound and transferring-bound iron uptake in primary hippocampal neurons

**Changyi Ji** and **Daniel J. Kosman***

Department of Biochemistry, State University of New York, School of Medicine and Biomedical Sciences Buffalo, NY 14214, USA

## Abstract

The molecular mechanisms of iron trafficking in neurons have not been elucidated. In this study, we characterized the expression and localization of ferrous iron transporters Zip8, Zip14 and DMT1, and ferrireductases Steap2 and SDR2 in primary rat hippocampal neurons. Steap2 and Zip8 partially co-localize, indicating these two proteins may function in $Fe^{3+}$ reduction prior to $Fe^{2+}$ permeation. Zip8, DMT1 and Steap2 co-localize with the transferrin receptor (TfR)/transferrin (Tf) complex, suggesting they may be involved in TfR/Tf-mediated iron assimilation. In brain interstitial fluid, transferring-bound iron (TBI) and non-transferrin-bound iron (NTBI) exist as potential iron sources. Primary hippocampal neurons exhibit significant iron uptake from TBI (Transferrin-$^{59}Fe^{3+}$) and NTBI, whether presented as $^{59}Fe^{2+}$-citrate or $^{59}Fe^{3+}$-citrate; reductase-independent $^{59}Fe^{2+}$ uptake was the most efficient uptake pathway of the three. Kinetic analysis of $Zn^{2+}$ inhibition of $Fe^{2+}$ uptake indicated that DMT1 plays only a minor role in the uptake of NTBI. In contrast, localization and knockdown data indicate that Zip8 makes a major contribution. Data suggest also that cell accumulation of $^{59}Fe$ from TBI relies at least in part on an endocytosis-independent pathway. These data suggest that Zip8 and Steap2 play a major role in iron accumulation from NTBI and TBI by hippocampal neurons.

### Keywords

primary hippocampal neurons; iron; Zip8; NTBI; TBI; ferrireductase; permease

## Introduction

Iron is essential to normal neuronal development and function. Robust energy metabolism and neurotransmitter synthesis are supported by enzymes that utilize iron as a cofactor (Altamura & Muckenthaler 2009). On the other hand, dysregulation of neuronal iron homeostasis correlates with reactive oxygen species (ROS) production and protein aggregation, in which the impacted brain regions exhibit cell damage and neural degeneration (Salazar *et al.* 2008, Moos & Morgan 2004a, Lee & Andersen 2010, Altamura

*To whom correspondence should be addressed: Daniel J Kosman, Department of Biochemistry, University at Buffalo, Farber Hall Room 140, 3435 Main St., Building 26, Buffalo, NY 14214-3000, USA.; (716) 829-2842; Fax: (716) 829-2661; camkos@buffalo.edu.

**conflict-of-interest disclosure**

The authors declare that they have no competing interests.

& Muckenthaler 2009, MacKenzie *et al.* 2008, Qian & Ke 2007, Zecca *et al.* 2004). Clearly, iron uptake, storage and export by neurons need to be both efficient and tightly regulated.

The molecular mechanisms of iron uptake in neurons have not been well characterized. Canonical transferrin receptor (TfR)-mediated transferring-bound iron (TBI) uptake is one potential pathway, in which iron is released as $Fe^{2+}$ from Tf in the acidic endosome in a reaction catalyzed by a putative ferrireductase, *e.g.* Steap3; the released $Fe^{2+}$ is transported into the cytosol through divalent metal transporter 1 (DMT1) (Ohgami *et al.* 2005). Neurons express TfR and DMT1 (Fretham *et al.* 2012, Siddappa *et al.* 2003, Siddappa *et al.* 2002, Haeger *et al.* 2010), suggesting they can acquire iron from TBI in the brain interstitial fluid. Estimation of total iron in cerebrospinal fluid (CSF) suggests that the iron concentration in the brain is 0.4–1.2 μM (Bleijenberg *et al.* 1971) or 0.3–0.75 μM (Gutteridge 1992), while the concentration of Tf is estimated to be 0.21–0.28 μM (Bleijenberg et al. 1971, Del Principe *et al.* 1989). In another study, the iron concentration in the brain was shown to exceed the binding capacity of transferrin found there (Moos & Morgan 1998), therefore, excess non-heme iron will be chelated by other low molecular weight ligands, such as citrate which, for example, is 175 μM in the CSF (Gaasch *et al.* 2007). As the composition of CSF is thought to be similar to that of the brain interstitial fluid, non-transferrin-bound iron (NTBI) is also a likely component in the brain interstitial fluid (Moos & Morgan 1998). Therefore, neurons are presented with both TBI and NTBI as potential sources of iron to fulfill their trophic needs; which source is used reasonably would depend on the expression of specific iron transport-related proteins in a given cell type.

DMT1 is a well characterized divalent iron transporter. It is expressed as four different isoforms as a result of differential transcription initiation and splicing at two alternative 3′ ends (Mackenzie *et al.* 2007, Tabuchi *et al.* 2002). Neurons express the 1B-DMT1 isoform (Haeger et al. 2010, Pelizzoni *et al.* 2012). 1B-DMT1 in neurons exhibits cytoplasmic (vesicular) distribution (Pelizzoni et al. 2012); this isoform functions at acidic pH with only limited activity at the physiologic (brain) pH of 7.4 (Pelizzoni et al. 2012, Mackenzie et al. 2007, Illing *et al.* 2012). Therefore, the role of DMT1 in neuronal NTBI uptake is unclear (Pelizzoni et al. 2012) and implicate of other ferrous iron transporters in neuronal iron uptake, a hypothesis that has yet to be tested. Members of the ZIP family of metal ion transporters, *e.g.* Zip8 and Zip14 (Wang *et al.* 2012, Pinilla-Tenas *et al.* 2011), are of particular interest. The transcripts of both Zip8 and Zip14 have been detected in mouse brain (Girijashanker *et al.* 2008, Wang *et al.* 2007). Exogenously expressed Zip8 and Zip14 possess plasma membrane localization in HepG2 and rat hepatoma cells (Liuzzi *et al.* 2006, Wang et al. 2012). The optimal pH of 7.5 for $Fe^{2+}$ and $Zn^{2+}$ permeation *via* Zip8 and Zip14 (Wang et al. 2012, Pinilla-Tenas et al. 2011) makes them good candidates to translocate $Fe^{2+}$ from the brain interstitial fluid into the neuronal cytosol.

Reduction of ferric iron is required for its uptake through a ferrous iron transporter. This process can be mediated by ferrireductases in living organisms. The Steap and cytochrome b561 families of metalloreductases are the only known mammalian ferrireductases (Anderson & Vulpe 2009, Ohgami *et al.* 2006, Vargas *et al.* 2003). The Steap family contains four members: Steap1, Steap2, Steap3 and Steap4; the last three exhibit ferrireductase activity (Ohgami et al. 2006, Ohgami et al. 2005). Steap2 mRNA has been

detected in the brain by in situ hybridization (Ohgami et al. 2006). The cytochrome b561 (Cyt b561) family includes chromaffin granule Cyt b561, lysosomal Cyt b561, duodenum Cyt b561 (Dcytb) and stromal cell derived receptor 2 (SDR2) (Vargas et al. 2003, Zhang *et al.* 2006, Tsubaki *et al.* 2005, Berczi *et al.* 2005, Wyman *et al.* 2008). Among these homologues, Cyt b561, Dcytb and SDR2 are functional ferrireductases (Oakhill *et al.* 2008, Vargas et al. 2003, Wyman et al. 2008). Dcytb and SDR2 transcripts have been detected in cultured rat astrocytes (Tulpule *et al.* 2010) and human brain endothelial cells (McCarthy & Kosman 2012); these two proteins likely contribute to extracellular ferric iron reduction before $Fe^{2+}$ permeation. This model has not been rigorously tested except for the well-established role of Dcytb in iron uptake by enterocytes. Neuronal expression of these or other ferrireductases has not been established nor has a ferrireduction-dependent mechanism in support of neuronal iron uptake from ferric NTBI.

In this study, we have characterized the expression and localization of Zip8, Zip14, Steap2 and SDR2 in primary hippocampal neurons. We demonstrate the co-localization of Zip8 and Steap2, and together with DMT1, co-localization with the TfR/Tf complex. $^{59}Fe$ uptake from all three potential iron sources – NTBI ($Fe^{2+}$-citrate, $Fe^{3+}$-citrate) and TBI ($Fe^{3+}$-transferrin) – was characterized in detail. The kinetics of metal competition of NTBI uptake by $Zn^{2+}$ suggests that Zip8 is a likely candidate for NTBI uptake; consistent with this hypothesis, Zip8 RNAi knock-down results in decreased $Fe^{2+}$ uptake. For TBI, endocytosis/endosomal acidification-insensitive Fe uptake was observed, suggesting a non-canonical mechanism supports iron accumulation from that source; we hypothesize some fraction of TBI Fe-uptake follows plasma membrane $Fe^{2+}$ release from TfR-bound Fe-Tf. In summary, we have quantified iron uptake by hippocampal neurons *in vitro*, providing evidence that Zip8 and Steap2 play major roles in this iron trafficking pathway.

## Materials and Methods

### Cell culture

Primary hippocampal neurons were prepared from D18 embryos carried by a Sprague Dawley dam (purchased from Harlan Laboratories, Indianapolis, IN) as previously described (Kaech & Banker 2006). All procedures were approved by the Institutional Animal Care and Use Committee of University at Buffalo. In brief, the hippocampus was removed and dissociated into a single cell suspension. These cells were plated on collagen and poly-D-lysine coated plates at a density of 5×104 cells/cm2. Cells were maintained in Neurobasal media supplemented with B27 and 0.5 μM L-glutamine (Gibco/Life Technologies, Grand Island, NY). On day 2 post plating, 1.5 μM AraC (Sigma-Aldrich, St. Louis, MO) was added to inhibit the proliferation of glial cells, resulting in relatively pure primary neuronal cultures (~98%) as indicated by immunostaining for MAP2 (neurons) and GFAP (glial cells). Ferrireductase and iron uptake assays employed neurons at 10–20 days post-plating except where noted.

### Total cell lysates and acetone precipitation

To prepare a total cell lysate, cells were washed twice with phosphate-buffered saline (PBS) and homogenized in ice-cold RIPA buffer (25 mM Tris, 150 mM NaCl, 1% NP-40, 1% Na-

deoxycholate, 0.1% SDS, pH 7.4) supplemented with protease inhibitors (1 mM PMSF and 1 μg/ml leupetin and pepstatin). To concentrate the protein extracts, 4 volumes of ice-cold acetone were added to each sample and the mixture was incubated at −20°C overnight. Protein pellets were collected and washed with ice-cold acetone twice by centrifugation at 14,000×g for 15 min at 4°C. After drying, the pellets were dissolved in Tris (pH 8.0) buffer containing 2% SDS. Protein concentration was measured by BCA assay (Thermo Scientific, Rockford, IL).

### Western blotting

Samples were denatured at 75°C for 10 min (SDR2 and Steap2) or 37°C for 30 min (DMT1, Zip8, and Zip14, TfR); samples (15 μg total protein/lane) were fractionated in 8% SDS-polyacrylamide gels, followed by transfer to a PVDF membrane. Membranes were blocked by TBST (Tris-buffered saline with 0.05% Tween-20) containing 5% BSA at 4°C for 1 hour. Primary antibodies were diluted in 1% BSA-TBST as follows: 1:6667 for rabbit anti-SDR2 antibody (Sigma-Aldrich, HPA017883), goat anti-Steap2 antibody (Santa Cruz Biotechnology, sc-82365), rabbit anti-Zip8 antibody (Sigma-Aldrich, SAB3500598) and rabbit anti-Zip14 antibody (Sigma-Aldrich, HPA016508); 1:5000 for rabbit anti-DMT1 (gift from Dr. Michael Garrick) and goat anti-TfR (R&D systems, AF2474). The blots were incubated at 4°C over night. After washing, membranes were incubated at room temperature for 1 h with secondary goat anti-rabbit or donkey anti-goat horseradish peroxidase conjugated antibodies (Santa Cruz Biotechnology), which were diluted 1:5000 in TBST containing 3% BSA. Immunocomplexes were visualized on film using SuperSignal West Dura Extended Duration Substrate (Thermo Scientific, Waltham, MA). Data on validation of antibodies used are provided in Fig. S2 and S3.

### Immunofluorescence

Neurons grown on coverslips were fixed in 4% paraformaldehyde, 4% sucrose in PBS for 10 min at room temperature, and blocked in 5% BSA with 0.3 M glycine in PBST (PBS with 0.5% Tween-20) for 45 min. Primary antibodies were diluted in PBS containing 1% BSA as follows: 1:200 for goat anti-TfR1; 1:500 for rabbit anti-SDR2, goat anti-Steap2, and rabbit anti-Zip14; and 1:1000 for mouse anti-microtubule-associated protein 2 (MAP2 Santa Cruz Biotechnology, sc-80013), rabbit anti-Zip8 and rabbit anti-DMT1 and then incubated with the cells at 4°C overnight. Alexa Fluor 647-conjugated donkey anti-rabbit or anti-goat IgG, and Alexa Fluor 488-conjugated donkey anti-mouse IgG (Life Technologies) were diluted 1:1000 and incubated with samples in the dark for 1 h at room temperature. After washing, samples were mounted onto slides with a drop of *SlowFade*® Gold Antifade Reagent containing DAPI (Invitrogen). The slides were visualized using either a LSM-510 Meta NLO laser scanning confocal microscope or Axioimager epifluorescence microscope (Zeiss). The images were processed in ImageJ and co-localization analyses were performed using JACoP plugins.

### RT-PCR and qPCR

Total RNA was prepared by using TRIzol reagent (Life Technologies), following manufacturer's instructions. DNase digestion (Thermo Scientific, Waltham, MA) was

performed before RNA clean up using the RNeasy Kit (Qiagen, Valencia, CA) to remove genomic DNA contamination. One-step RT-PCR was performed using the QIAGEN®OneStep RT-PCR Kit and analyzed on agarose gels. Primers spanning two exons and targeting the mRNA sequence of each protein were as follows: Zip8, forward, 5′-ACGTCACCCAGATAACCAGC-3′, reverse, 5′-CAAGAATCCATAGCCCCAGAC-3′; Zip14, forward, 5′-GAAGCAGAAAAACGAGCACC-3′, reverse, 5′-CCCTTTGAGCCAGTAGCAAG-3′; 1B-DMT1, forward, 5′-CAATCACGGGAGGGCAGGAG-3′, reverse, 5′-AGGTAGGCAATGCTCATAAGAAAACCAGG-3′ (Haeger et al. 2010); Steap2, forward, 5′-GGCTTATCAGGTGCGGCTATC-3′, reverse, 5′-GGCTGACGACAAAGATCCCAAG-3′; SDR2 forward, 5′-TCGCACTTAACCAAACCATTC-3′, reverse, 5′-GTGAAGGACAAGAAGACGCAG-3′. For qPCR, first strand cDNAs were synthesized from 500 ng total RNA using the iScript cDNA synthesis kit (Bio-rad, Hercules, CA). Real-time quantitative PCR was performed by using SsoAdvanced™ Universal SYBR® Green Supermix and analyzed on a CFX96 Touch™ Real-Time PCR Detection System (Bio-rad, Hercules, CA). Relative expression of target mRNA was normalized to GAPDH mRNA expression by calculating the $\Delta\Delta C_t$ value.

## Ferrireductase activity assay

Primary hippocampal neurons were washed three times with pre-warmed physiological incubation buffer (PIB - 25 mM MOPS, 25 mM MES, 5 mM glucose, 140 mM NaCl, 5.4 mM KCl, 1.8 mM $CaCl_2$, 0.8 mM $MgCl_2$, pH 7.2). NTBI was prepared with 50 μM $FeCl_3$ and either 200 μM nitrilotriacetic acid (NTA), or 1 mM citrate. In the presence of 1mM ferrozine, 50 μM NTBI or 25 μM TBI (holo-Tf, Calbiochem) was added to the neuronal culture in PIB buffer. Ferrireduction was calculated from absorbance increase at 562 nm due to formation of the $Fe^{2+}$-ferrozine complex; $Fe^{2+}$ generation was calculated with reference to a $Fe^{2+}$-ferrozine standard curve, and normalized to the total amount of protein in each well.

## Iron uptake assay

Cells were washed three times with uptake buffer (PIB without $Ca^{2+}$ and $Mg^{2+}$), then incubated in uptake buffer for 15 min at 37°C followed by an additional wash to remove endogenous Tf. $^{59}FeCl_3$ (Perkin Elmer, Waltham, MA) was mixed with citrate (at a ratio of 1: 200) in uptake buffer to make a $^{59}Fe^{3+}$-citrate stock. $^{59}Fe^{3+}$-citrate was added in uptake buffer with ($^{59}Fe^{2+}$-citrate) or without ($^{59}Fe^{3+}$-citrate) 5 mM ascorbate. For TBI uptake, $^{59}FeCl_3$ was loaded into apo-transferrin (Sigma-Aldrich, St. Louis, MO) following a published method (McCarthy & Kosman 2012); $^{59}Fe^{3+}$-transferrin was added to each cell culture to a final [Tf] = 0.5 μM (1 μM total Fe). Cells were incubated at 37°C for 20 min for NTBI uptake, or 1 hour for TBI uptake, unless noted. Cells were washed four times using ice-cold quenching buffer (uptake buffer containing 1 mM EDTA, pH7.4 for NTBI uptake, pH5.5 for TBI uptake) and harvested in RIPA buffer (50 mM Tris, 150 mM NaCl, 1.0% IGEPAL® CA-630, 0.5% sodium deoxycholate, 0.1% SDS, pH 8.0.). $^{59}Fe$ accumulated in each sample was measured using an LKB Wallac CompuGamma counter. The amount of $^{59}Fe$ uptake in each sample was quantified and normalized to protein content as determined by BCA assay.

### Lentiviral transduction and RNA interference (RNAi)

A lentiviral system was used to deliver a short-hairpin RNA (shRNA) into primary hippocampal neurons. The Zip8 targeting siRNA sequence was 5′-GTCAAGTTCATGCACCTGTTT-3′ (Sigma MISSION). A scrambled sequence (5′-CCTAAGGTTAAGTCGCCCTCG-3′) was used as non-target control. The shRNA oligonucleotides were ligated into lentiviral vector pLKO.3G (Addgene). The resulting vector (10 μg) was co-transfected with packaging plasmids pMD2.G (3 μg) and psPAX2 (7 μg) (Addgene) into HEK293T/17 cells to produce the lentivirus. Media containing lentiviral particles was collected at 36, 48 and 60 hours post transfection, filtered through 0.45 μm filters, and concentrated by ultracentrifugation. The titers were estimated in HEK293T cells. Primary cultured hippocampal neurons at day 6 post plating were infected with shRNA lentivirus at MOI of 20 to achieve >90% infection. At 8–10 days post infection, the efficiency of Zip8 knockdown was tested by real-time PCR and immunoblot analysis.

### Data analyses

Data are presented as mean ±SD. Statistical analyses were performed using GraphPad Prism 5 (GraphPad Software, San Diego, CA, USA). The Michaelis-Menten equation was fitted to *v versus* [$^{59}$Fe] uptake data. An equation describing simple competitive inhibition was fitted to the complete data set describing $Zn^{2+}$ inhibition. Linear regression analysis was used to analyze rate data in reciprocal form. Statistical significance was tested by either unpaired t test or one-way ANOVA followed by Bonferroni pair-wise comparison *post hoc* test when noted. In the text, “n =” refers to the number of technical replicates used to derive the stated quantity; where appropriate the number of experimental replicates are given as well.

## Results

### Ferrous iron transporters (Zip8, Zip14 and DMT1), ferrireductases (Steap2 and SDR2) and TfR are expressed by primary hippocampal neurons

The expression of mammalian iron uptake transporters Zip8, Zip14 and 1B-DMT1 was detected at the mRNA level in primary hippocampal neurons (Fig. 1a). Uptake of ferric iron species by these divalent metal ion transporters is preceded by ferrireduction. Thus, neuronal expression of genes encoding such ferrireductases was evaluated also, *e.g.* members of the Steap and cytochrome b561 families of ferrireductases. Among the members of the Steap family, Steap2 appears in relatively high expression in the brain, compared to the other members (Ohgami et al. 2006). We detected neuronal expression of Steap2 (Fig. 1b and 1d), but not Steap3 (data not shown). The expression of Dcytb, which has been detected in primary astrocytes (Tulpule et al. 2010), was not detected by our RT-PCR analysis (data not shown). In contrast, the expression of SDR2, another member of the cyt b561 family, was detected at the mRNA level (Fig. 1b).

Polyclonal antibodies directed towards Zip8, Zip14 or the N-terminal sequence of DMT1 exon2, detected Zip8 at ~50 and 100 kDa, Zip14 at ~54 and 150 kDa, and a major band of DMT1 at ~60 kDa in Western blot analysis of neuronal cell extracts; thus all three divalent metal ion transporters are expressed at the protein level (Fig. 1c). Western blot analysis of cell extracts derived from neurons as a function of time in culture demonstrated a consistent

expression of all three proteins throughout the process of neuronal differentiation; the same was true of Steap2 (Fig. 1d). In contrast, at the protein level, SDR2 expression increased in the neuronal culture as a function of days post-plating. TfR, which is essential for iron uptake from transferrin, was expressed at a constant level (Fig. 1e).

## Cellular localization of Zip8, Zip14, Steap2 and SDR2 in primary hippocampal neurons

TfR and DMT1 have a punctate intracellular localization in primary neurons (Burdo *et al.* 2001, Moos & Morgan 2004b), but no data have been published in regards to the localization of the other four proteins in this cell type. Thus, we performed indirect immunofluorescence confocal microscopy to determine the cell locale of Zip8, Zip14, Steap2 and SDR2. MAP2, enriched in neuronal dendrites, is an intracellular neuronal specific marker. Zip8 was detected mainly at the cell surface of the soma and dendrites (Fig. 2a). In contrast, Zip14 exhibited both cytosolic localization and nuclear staining (Fig. 2a). Steap2 was visualized in both the plasma membrane and the cytosol, while SDR2 localized to the plasma membrane (Fig. 2b). On the basis of this localization pattern, we suggest that SDR2 or Steap2 could be responsible for ferric iron reduction at the cell surface and that Zip8 could support ferrous iron permeation. In contrast, Steap2 and Zip14 could contribute primarily to iron trafficking associated with subcellular compartments.

To interrogate which iron transporter(s) is likely involved in TBI uptake, we investigated the possible proximity of the iron transporters Zip8, Zip14 and DMT1 to TfR/Tf by co-localization analyses (Fig. 3a). The data showed a distinct co-localization of TfR and Zip8 in the plasma membrane of neuronal soma and processes; TfR and DMT1 appear to have a similar, but a stronger co-localization on neuronal processes. In contrast, only a weak intracellular co-localization of TfR and Zip14 in neuronal soma was observed. Since TfR is internalized upon binding to its ligand Tf, we tested whether the spatial localization between TfR and an iron transporter changed upon Tf binding. Therefore, the co-localization analyses of Tf and the three iron transporters was also carried out in the presence of added holo-Tf; in these experiments we took advantage of the Tf-Alexa Fluor 594 reagent (Tf-594) (Fig. 3b). In a 5 min incubation, the internalized Tf-594 co-localized with Zip8 in neuronal processes but with DMT1 in neuronal soma, respectively. In contrast, a minimal co-localization of Tf-594 and Zip14 was observed.

We examined also the potential co-localization of ferrireductase and iron transporter proteins. Indeed, a strong co-localization of Steap2 and Zip8 on the cell surface of soma and dendrites was observed (Fig. 4a). This co-localization suggests that these two proteins may function together to support non-transferrin bound ferric iron reduction and uptake in primary hippocampal neurons. To test which ferrireductase(s) may participate in transferrin bound ferric iron reduction, we investigated the spatial proximity between Steap2 or SDR2 and internalized Tf-594 as above. Co-localization of both Steap2 and SDR2 with Tf-594 was observed (Fig. 4b). This result suggests either or both ferrireductases could be associated with TBI uptake $^{59}$Fe-uptake in primary hippocampal neurons.

Previous data has demonstrated that non-transferrin bound iron (NTBI) as ferrous iron can be directly transported into neurons (Cheah *et al.* 2006, Pelizzoni *et al.* 2011, Pelizzoni et al. 2012). Our objective was to characterize this uptake in kinetic detail and thus be able to

delineate the divalent metal ion transporter or transporters associated with this ferrous iron accumulation. In our neuronal cultures, radioactive $^{59}Fe^{2+}$ uptake (presented as $Fe^{2+}$-citrate) was time- and temperature-dependent; uptake was linear for at least 10 min (Fig. 5a). In our protocol, the amount of cell-associated iron detected at 4°C is quantitatively the same as the amount detected in 37° C cells at t = 0 (time relative to the addition of the radionuclide); this value was taken to represent non-specific, cell-associated iron. Our data show also that $^{59}Fe^{2+}$ uptake in primary hippocampal neurons behaves as a saturable kinetic process (Fig. 5b). Fitting the Michaelis-Menten equation to these data provided values for $K_m$ (6.0 ± 1.0 μM) and $V_{max}$ (92 ± 7 pmol Fe/mg protein/min).

We also examined the kinetics of $Fe^{3+}$-citrate uptake in our primary hippocampal neuron model system. $^{59}Fe^{3+}$-citrate uptake in primary hippocampal neurons also was time- and temperature-dependent (Fig. 5c). Note that at [Fe] = 1 μM the initial velocity of $^{59}Fe^{3+}$ uptake (Fig. 5c) was much slower in comparison to uptake of $^{59}Fe$ from $Fe^{2+}$-citrate (Fig. 5a), a difference which reasonably is due to the ferrireduction step that in uptake from a ferric iron species precedes the actual permeation of iron in its ferrous redox state. Nonetheless, the uptake of $^{59}Fe$ from $Fe^{3+}$-citrate appeared to exhibit saturation kinetics, also (Fig. 5d); a fit of the Michaelis-Menten equation to the uptake data yielded values for $K_m$ (0.09 ± 0.03 μM) and $V_{max}$ (25.5 ± 1.4 pmol Fe/mg protein/min). Note, however, that given the apparent value for $K_M$ (~0.1 μM) this analysis is limited by the lack of velocity data obtained at [Fe] < $K_M$.

Another potential ferric iron source in brain interstitial fluid is transferrin bound $Fe^{3+}$, TBI. To test the efficiency of $^{59}Fe^{3+}$ uptake from TBI by primary hippocampal neurons, we performed a time course assay as above, demonstrating that $^{59}Fe$ uptake from TBI exhibits a time- and temperature-dependence (Fig. 5e) that, in comparison to NTBI accumulation, showed TBI $^{59}Fe$ uptake to be quantitatively slower than ferrous iron, but similar to ferric iron. Note that in this experiment (Fig. 5e), the Tf concentration was chosen to yield the same [Fe] (1.0 μM) used to examine the time dependence of iron uptake from $Fe^{2+}$-citrate (Fig. 5a) and from $Fe^{3+}$-citrate (Fig. 5c).

## NTBI $^{59}$Fe-uptake can be inhibited by other divalent metal ions

59Fe2+ uptake in primary hippocampal neurons was inhibited by Zn2+, Mn2+ and Cd2+ (Fig. 6a). Zn2+ was the most efficient inhibitor of 59Fe2+ uptake, followed by Cd2+ and Mn2+. To investigate the mechanism of zinc inhibition, we performed a kinetic analysis of 59Fe2+ uptake in the presence of varying [Fe2+] and (Illing et al. 2012, Garrick et al. 2006b)[Zn2+]. The measured 59Fe2+ uptake rates are given in reciprocal form in Fig. 6b; the lines represent the fit of the Michaelis-Menten equation to the uptake rates at each [Zn2+] providing apparent Km (app) values for Fe2+. These values were then replotted as function of [Zn2+] (Fig. 6c) providing visual evidence that Zn2+ is a competitive inhibitor of Fe2+ uptake. Fitting an equation representing simple competitive inhibition to all of the rate data provided the Ki value for Zn2+, 7.6 μM, a value comparable to the reported Km of 65Zn2+ uptake in hippocampal neurons (Colvin et al. 2008), and the Km of Zn2+ uptake via either Zip8 or Zip14 (Liuzzi et al. 2006, Wang et al. 2012). Since DMT1 exhibits a Km for Zn2+ uptake of 32 μM, and a Ki for Zn2+ inhibition of Fe2+ uptake of 26 μM (or an IC50

value of 180.3 μM), our results are consistent with a previous report that DMT1 makes a limited contribution to Fe2+ uptake in primary hippocampal neurons (Pelizzoni et al. 2012).

$^{59}Fe^{3+}$-citrate uptake was also inhibited by $Zn^{2+}$ (Fig. 6d). This result is consistent with the model that $Zn^{2+}$ competes for uptake with the ferrous iron product of the ferrireduction step required for neuronal accumulation of $Fe^{3+}$ from an NTBI source. Indeed, ferrireductase activity is present in hippocampal neurons (Fig. 6e). Based on the cell localization data presented above, this cell surface reductase activity could be due to SDR2 and/or Steap2. Note that the data in Fig. 6e indicate that in contrast to the active reduction of NTBI ($Fe^{3+}$-citrate and $Fe^{3+}$-NTA), hippocampal neurons exhibit a more limited efficiency in the reduction of TBI (Tf-$Fe^{3+}$).

### Zip8 functionally supports $Fe^{2+}$ uptake in primary hippocampal neurons

The cell surface localization of Zip8, together with the $Zn^{2+}$ inhibition data suggest Zip8 makes a significant contribution to NTBI uptake in primary hippocampal neurons. To test this hypothesis, a lentiviral shRNA delivery system was used to knockdown the endogenous Zip8 transcript. The transcript abundance of Zip8 was decreased by 50% in this Zip8 shRNA knockdown experiment (Fig. 7a), which resulted in an equivalent reduction of Zip8 protein expression (Fig. 7b). Significantly, $^{59}Fe^{2+}$ uptake was decreased proportionally in these Zip8 knockdown neurons in comparison to the control (Fig. 7c). These results are consistent with a model that Zip8 plays an important if not major role in $Fe^{2+}$ accumulation from NTBI in hippocampal neurons at physiological pH.

### $^{59}$Fe uptake from TBI ($^{59}$Fe-Tf) in primary hippocampal neurons is not linked to endocytosis nor endosomal acidification

The strong co-localization of Zip8 and TfR/Tf on the cell surface suggested that TBI uptake in these neurons relied on some non-canonical mechanism, that is, one that was independent of the endosomal trafficking of the TfR-Tf complex. To further examine TBI uptake, we examined the role of endocytosis in $^{59}$Fe uptake from $^{59}$Fe-Tf. First, we demonstrated endocytosis of Tf-594 and showed that it was inhibited by dynasore, an inhibitor of dynamin whose function is required for the cycling of clathrin-coated vesicles (Fig. 8a). Significantly, despite the block of Tf internalization by dynasore, dynasore had no significant effect on $^{59}$Fe uptake from TBI (Fig. 8b). In addition, acidification of the endosome also was not required for $^{59}$Fe accumulation from $^{59}$Fe-Tf; neither bafilomycin A1 nor concanamycin A, two ATPase/$H^+$ pump inhibitors, had any statistically significant effect on $^{59}$Fe uptake from TBI. A similar negative result was observed in the presence of the alkalization reagent $NH_4Cl$ (Fig. 8c).

## Discussion

Neuronal iron homeostasis requires a balance between iron import, storage and efflux. Our objective here was to fully characterize iron uptake into primary hippocampal neurons. In addition to the well-characterized TfR and DMT1 (Fretham et al. 2012, Pelizzoni et al. 2012, Haeger et al. 2010), we investigated also the expression and function of ferrireductases, Steap2 and SDR2, and two other ferrous iron transporters, Zip8 and Zip14;

the role(s) of these last four proteins in neuronal iron metabolism have not been examined previously.

Our biochemical results confirm that 1B-DMT1 is expressed in primary hippocampal neurons and has an intracellular localization (Pelizzoni et al. 2012, Haeger et al. 2010). Since DMT1 mediates a relatively low affinity $Zn^{2+}$ transport (Illing et al. 2012, Garrick *et al.* 2006a, Garrick et al. 2006b), the high affinity $Zn^{2+}$ inhibition of $Fe^{2+}$ (NTBI) uptake in these cultured neurons indicates that DMT1 likely is not a major iron transporter of NTBI *in vitro*. However, we can't rule out the possibility that other DMT1 isoforms in another, perhaps pathological, condition, *e.g.* MPTP-induced Parkinsonism, may contribute to iron accumulation in neurons (Salazar et al. 2008). Another possibility is that signaling linked to NMDA receptor activation could modulate the cell locale and/or function of DMT1, thus resulting in an increase in DMT1-dependent $Fe^{2+}$ uptake (Cheah et al. 2006).

Zip14 and Zip8, two ZIP family members, were recently identified as mammalian iron transporters in addition to their function in zinc import (Wang et al. 2012, Liuzzi et al. 2006). We detected the expression of Zip8 and Zip14 at both the transcript and protein level in our cultures. In non-CNS cells, plasma membrane and endosomal localization of Zip8 has been observed in HEK293T cells expressing Zip8 and in lung epithelia (Wang et al. 2012, Besecker *et al.* 2008). Zip14 exhibits partial co-localization with early and late endosome markers in HepG2 cells (Pinilla-Tenas et al. 2011, Zhao *et al.* 2010). The nuclear localization of Zip14 has been reported in the hair cells of rat inner ear (Ding *et al.* 2014). In primary hippocampal neurons, we observed Zip8 localization primarily at the plasma membrane. In contrast, Zip14 demonstrated only intracellular localization, primarily in neuronal soma, with strong nuclear staining as well. These observations suggest Zip8 and Zip14 have different roles in handling iron trafficking in these cells.

Our co-localization analyses of Zip8, Zip14 and DMT1 with TfR/Tf linked all three iron transporters to the TfR/Tf cycle. Of particular interest, we observed strong co-localization between Zip8 and TfR/Tf, especially near the cell surface of neuronal soma and processes. This co-localization of Zip8 and TfR/Tf has not been reported before. On the other hand, Zip14, a closely related homologue of Zip8, exhibits partial co-localization with Tf, TfR, early endosomal marker EEA1, and late endosomal marker LAMP1 in HepG2 cells (Zhao et al. 2010). Our results were somewhat different in that we observed only moderate intracellular co-localization of Zip14 and TfR, and even weaker co-staining of Zip14 and. This pattern suggests a limited role for Zip14 in neuronal iron assimilation from TBI. Our data, however, do not provide any clue as to what role Zip14 may play in these cells. We did observe co-localization between DMT1 and TfR in these neurons, which is in agreement with some data (Tabuchi *et al.* 2010) but not with other observations (Pelizzoni et al. 2012); the latter report noted that the major neuronal DMT1 form, 1B-DMT1+IRE, did not co-localize with TfR/EEA1 in primary hippocampal neurons. Perhaps in contrast with that conclusion is our strong evidence for Tf-564, DMT1 co-trafficking which supports the role of DMT1 in TfR/Tf cycling that has been widely accepted.

Ferrireductases can support $Fe^{3+}$ reduction thus supplying $Fe^{2+}$ substrate for permeation through divalent metal ion transporters such as Zip8, Zip14 and DMT1. This reduction of

dietary non-heme iron at duodenum brush boarder is mediated by Dcytb (Wyman et al. 2008, Latunde-Dada *et al.* 2008, McKie *et al.* 2001); TBI in the endosome of erythrocytes is reduced by Steap3 (Lambe *et al.* 2009, Ohgami et al. 2005). Among all the members of the Steap and Cytochrome b561 families of ferrireductases, transcripts for Dcytb, SDR2 and Steap2 have been detected in the brain (Vargas et al. 2003, Ohgami et al. 2006, Tulpule et al. 2010). In primary hippocampal neurons, we detected only Steap2 and SDR2 at the transcript and protein levels.

The distinct localization of Steap2 and SDR2 that we report suggest that these two reductases contribute to iron trafficking in different cell locales. The expression of Steap2 at the cell surface and its strong intracellular co-localization with TfR/Tf have been shown in Steap2-expressing HEK293 cells (Ohgami et al. 2006). Consistently, we observed Steap2 at the cell surface where it co-localizes with Zip8; this pattern suggests a model in which Steap2 supports extracellular NTBI reduction followed by permeation *via* Zip8. The co-localization between Steap2 and internalized Tf was observed also, suggesting that Steap2 may be the ferrireductase involved in TBI reduction in this cell type, as well. SDR2 localized to the plasma membrane also and exhibited some internalization with Tf-564. These data suggest that SDR2 may provide a redundant function in both NTBI and TBI ferrireduction.

In brain interstitial fluid (ISF), iron could be bound to transferrin, lactoferrin or ferritin (Gaasch et al. 2007), although the concentration of these proteins in the SIF is low, *e.g.* the concentration of Tf (0.21–0.28 μM) in the brain is far less than that in systemic circulation (~25 μM) (Bradbury 1997, Gaasch et al. 2007). Lactoferrin (Lf) has been reported at ~0.075 nM in CSF (Fillebeen *et al.* 1999). Lf-mediated iron delivery is through lactoferrin receptor (LfR); LfR expression has been detected in a variety of cell types including neurons in mesencephalon, where the TfR expression is relatively low (Faucheux *et al.* 1995). CSF ferritin is at an even lower concentration (~6.67 pM) (Burdo & Connor 2003). Although ferritin can deliver iron into oligodendrocytes in a receptor-mediated process (Todorich *et al.* 2011), there is no evidence available concerning ferritin receptor expression in neurons.

The differential between the concentrations of brain non-heme iron (~1 μM) and Tf (~0.25 μM) indicates that low molecular mass iron ligands do have access to “free” iron, *e.g.* citrate. The existence of NTBI in the ISF has been reported in several studies (Bradbury 1997, Moos & Morgan 1998, Savman *et al.* 2005, McCormick *et al.* 2013). However, the composition of iron species in this NTBI pool has not been delineated and in any event would be complicated by dynamic redox cycling and ligand exchange reactions. With the high level of ascorbate and low level of soluble ceruloplasmin in human CSF as a guide (Gutteridge 1992), NTBI could exist in both the ferrous and ferric iron state. A recent study estimated the mononuclear non-heme iron content in mouse brain, *i.e.* $Fe^{2+}$ at ~20 μM and $Fe^{3+}$ at ~300 nM (Holmes-Hampton *et al.* 2012). The fraction of this iron that resides in the ISF specifically would presumably be available for neuronal iron accumulation suggesting that $Fe^{2+}$ predominates over $Fe^{3+}$ as a potential substrate.

We have shown that primary hippocampal neurons can accumulate iron from $^{59}Fe^{2+}$-citrate, $^{59}Fe^{3+}$-citrate and $^{59}Fe^{3+}$-transferrin. In our time-dependent iron uptake assay with

substrates presented to the cells at the same [Fe] = 1 μM, the initial rate of iron uptake from $^{59}Fe^{2+}$-citrate is faster than from $^{59}Fe^{3+}$-citrate or $^{59}Fe^{3+}$-transferrin, which suggests ferrous iron uptake is more efficient than for either ferric species. However, while the maximal velocity ($V_{max}$) of $^{59}Fe^{2+}$-citrate uptake is more robust than that of $^{59}Fe^{3+}$-citrate uptake, comparison of $V_{max}/K_m$ values (16.6 for $^{59}Fe^{2+}$-citrate and 283.3 for $^{59}Fe^{3+}$-citrate) suggests that the iron uptake efficiency may be higher when $Fe^{3+}$-citrate is the substrate. In summary, both ferrous and ferric iron, presented as a citrate complex (Pelizzoni et al. 2011, Bradbury 1997), appear to be kinetically competent iron sources for hippocampal neurons.

We took advantage of metal competition to interrogate a possible role for a ZIP transporter in neuronal iron uptake. Zip8 and Zip14 exhibit broad substrate profiles with varying affinity for different metal ion substrates (Illing et al. 2012, Wang et al. 2012, Pinilla-Tenas et al. 2011). Indeed, $Zn^{2+}$ competitively inhibited $Fe^{2+}$ uptake in hippocampal neurons with a $K_i$ value for $Zn^{2+}$ inhibition of $Fe^{2+}$ uptake that was comparable to the $K_m$ of neuronal $Zn^{2+}$ uptake (Colvin et al. 2008). $Fe^{2+}$, $Zn^{2+}$ and $Mn^{2+}$ are substrates for both Zip8 and Zip14 (Wang et al. 2012, Girijashanker et al. 2008, Liu *et al.* 2008). Zip8 transports these metals with affinity constants in the order of $Zn^{2+} > Fe^{2+} > Mn^{2+}$ (Wang et al. 2012). Consistently, we observed that $Zn^{2+}$ was a more efficient inhibitor of $Fe^{2+}$ uptake than $Mn^{2+}$. Also, the optimum pH for Zip8-dependent uptake is 7.5 (Wang et al. 2012); therefore, Zip8 is an appropriate candidate transporter for neuronal iron uptake given that the pH of the ISF is 7.2 (Moos & Morgan 2004a). Indeed, our shRNA knockdown results, together with the unique Zip8 surface localization, provide direct evidence in support of our model that Zip8 is a primary ferrous iron transporter in primary hippocampal neurons.

$Fe^{3+}$-citrate, likely a major form of ferric NTBI, is an excellent substrate for iron uptake, as discussed above. Iron accumulation from this substrate also was strongly inhibited by $Zn^{2+}$ suggesting that iron from the ferric citrate complex and $Zn^{2+}$ compete, likely at the level of uptake. Since no mammalian ferric iron transporter has been characterized so far, it is more likely $Fe^{2+}$-citrate - as the ferrous iron product of ferrireduction - and $Zn^{2+}$ compete for a divalent metal transporter. Again, Zip8 is the likely candidate for the uptake of this NTBI form because of its localization (compared to Zip14) and affinity for $Zn^{2+}$ (compared to DMT1). $Fe^{3+}$ reduction following $Fe^{2+}$ permeation has been proposed as the mechanism of NTBI uptake in mammalian cells (Sturrock *et al.* 1990, Inman & Wessling-Resnick 1993, Oshiro *et al.* 1993). This model is supported by the fact that ferrous iron chelators BPS and ferrozine inhibit the cell accumulation of iron presented in the ferric form (Lane *et al.* 2010, Tulpule et al. 2010, Thorstensen & Romslo 1988, Thorstensen 1988).

Our TBI uptake data provide novel insights as to the role of endocytosis in iron assimilation from TBI by primary hippocampal neurons. Consistent with a previous report (Macia *et al.* 2006), we observed Tf-564 trafficking associated with endocytosis, a process blocked by dynasore. However, the release and uptake of iron from TBI was not markedly inhibited by treatment with this dynamin inhibitor indicating that iron accumulation from TBI was not solely dependent on endocytosis (and endosomal acidification); similar data have been provided by studies in hepatocytes and erythrocytes (Thorstensen 1988, Thorstensen & Romslo 1988, Oshiro et al. 1993). Based on our co-localization data, we propose that canonical endocytosis-dependent TBI uptake depends on DMT1 and Steap2 whereas the

apparently more robust, endocytosis-independent iron accumulation from TBI could rely on Steap2 and Zip8 functioning at or near the cell surface of neuronal processes. SDR2 may also contribute to ferrireduction in these uptake pathways. Clearly, additional functional tests on neurons carrying knock-downs of the individual proteins need to be done to test this model.

In conclusion, we report that primary hippocampal neurons express ferrous iron transporters, Zip8 and Zip14, and ferrireductases, SDR2 and Steap2, in addition to the known neuronal iron transport proteins, DMT1 and TfR. Our results provide evidence that Zip8 contributes to $Fe^{2+}$ uptake; the role of DMT1 (and Zip14) in NTBI accumulation by primary hippocampal neurons is limited under normal physiological conditions (Pelizzoni et al. 2012). In addition to canonical DMT1-associated endocytosis-mediating TBI uptake, $Fe^{3+}$ uptake in these cells from either TBI or NTBI may occur through the Steap2-mediated ferrireduction at the cell surface coupled to Zip8-mediated $Fe^{2+}$ permeation.

## Supplementary Material

Refer to Web version on PubMed Central for supplementary material.

## Acknowledgments

We thank Dr. Wade Sigurdson for assistance in the use of the Confocal Microscopy and Flow Cytometry Facility in the School of Medicine and Biomedical Sciences, University at Buffalo. We also thank Dr. Michael Garrick for providing us with DMT1 antibody. This work was supported by Grant DK053820 from the National Institutes of Health to DJK.

## Abbreviations used

| | |
|---|---|
| **NTBI** | non-transferrin bound iron |
| **TBI** | transferrin bound iron |
| **Tf** | transferrin |
| **TfR1** | transferrin receptor 1 |
| **DMT1** | divalent metal transporter 1 |
| **CSF** | cerebrospinal fluid |
| **ISF** | interstitial fluid |

## References

Altamura S, Muckenthaler MU. Iron toxicity in diseases of aging: Alzheimer's disease, Parkinson's disease and atherosclerosis. Journal of Alzheimer's disease : JAD. 2009; 16:879–895.

Anderson GJ, Vulpe CD. Mammalian iron transport. Cell Mol Life Sci. 2009; 66:3241–3261. [PubMed: 19484405]

Berczi A, Su D, Lakshminarasimhan M, Vargas A, Asard H. Heterologous expression and site-directed mutagenesis of an ascorbate-reducible cytochrome b561. Archives of biochemistry and biophysics. 2005; 443:82–92. [PubMed: 16256064]

Besecker B, Bao S, Bohacova B, Papp A, Sadee W, Knoell DL. The human zinc transporter SLC39A8 (Zip8) is critical in zinc-mediated cytoprotection in lung epithelia. American journal of physiology. Lung cellular and molecular physiology. 2008; 294:L1127–1136. [PubMed: 18390834]

Bleijenberg BG, Van Eijk HG, Leijnse B. The determination of non-heme iron and transferrin in cerebrospinal fluid. Clinica chimica acta; international journal of clinical chemistry. 1971; 31:277–281.

Bradbury MW. Transport of iron in the blood-brain-cerebrospinal fluid system. J of Neurochem. 1997; 69:443–454. [PubMed: 9231702]

Burdo JR, Connor JR. Brain iron uptake and homeostatic mechanisms: an overview. Biometals : an international journal on the role of metal ions in biology, biochemistry, and medicine. 2003; 16:63–75.

Burdo JR, Menzies SL, Simpson IA, Garrick LM, Garrick MD, Dolan KG, Haile DJ, Beard JL, Connor JR. Distribution of divalent metal transporter 1 and metal transport protein 1 in the normal and Belgrade rat. Journal of neuroscience research. 2001; 66:1198–1207. [PubMed: 11746453]

Cheah JH, Kim SF, Hester LD, Clancy KW, Patterson SE 3rd, Papadopoulos V, Snyder SH. NMDA receptor-nitric oxide transmission mediates neuronal iron homeostasis via the GTPase Dexras1. Neuron. 2006; 51:431–440. [PubMed: 16908409]

Colvin RA, Bush AI, Volitakis I, Fontaine CP, Thomas D, Kikuchi K, Holmes WR. Insights into $Zn^{2+}$ homeostasis in neurons from experimental and modeling studies. Am J Physiol Cell Physiol. 2008; 294:C726–742. [PubMed: 18184873]

Del Principe D, Menichelli A, Colistra C. The ceruloplasmin and transferrin system in cerebrospinal fluid of acute leukemia patients. Acta paediatrica Scandinavica. 1989; 78:327–328. [PubMed: 2929361]

Ding D, Salvi R, Roth JA. Cellular localization and developmental changes of Zip8, Zip14 and transferrin receptor 1 in the inner ear of rats. Biometals : an international journal on the role of metal ions in biology, biochemistry, and medicine. 2014; 27:731–744.

Faucheux BA, Nillesse N, Damier P, et al. Expression of lactoferrin receptors is increased in the mesencephalon of patients with Parkinson disease. Proceedings of the National Academy of Sciences of the United States of America. 1995; 92:9603–9607. [PubMed: 7568181]

Fillebeen C, Descamps L, Dehouck MP, Fenart L, Benaissa M, Spik G, Cecchelli R, Pierce A. Receptor-mediated transcytosis of lactoferrin through the blood-brain barrier. J Biol Chem. 1999; 274:7011–7017. [PubMed: 10066755]

Fretham SJ, Carlson ES, Wobken J, Tran PV, Petryk A, Georgieff MK. Temporal manipulation of transferrin-receptor-1-dependent iron uptake identifies a sensitive period in mouse hippocampal neurodevelopment. Hippocampus. 2012; 22:1691–1702. [PubMed: 22367974]

Gaasch JA, Lockman PR, Geldenhuys WJ, Allen DD, Van der Schyf CJ. Brain iron toxicity: differential responses of astrocytes, neurons, and endothelial cells. Neurochemical research. 2007; 32:1196–1208. [PubMed: 17404839]

Garrick MD, Kuo HC, Vargas F, Singleton S, Zhao L, Smith JJ, Paradkar P, Roth JA, Garrick LM. Comparison of mammalian cell lines expressing distinct isoforms of divalent metal transporter 1 in a tetracycline-regulated fashion. The Biochemical journal. 2006a; 398:539–546. [PubMed: 16737442]

Garrick MD, Singleton ST, Vargas F, et al. DMT1: which metals does it transport? Biol Res. 2006b; 39:79–85. [PubMed: 16629167]

Girijashanker K, He L, Soleimani M, Reed JM, Li H, Liu Z, Wang B, Dalton TP, Nebert DW. Slc39a14 gene encodes ZIP14, a metal/bicarbonate symporter: similarities to the ZIP8 transporter. Molecular pharmacology. 2008; 73:1413–1423. [PubMed: 18270315]

Gutteridge JM. Ferrous ions detected in cerebrospinal fluid by using bleomycin and DNA damage. Clinical science. 1992; 82:315–320. [PubMed: 1372200]

Haeger P, Alvarez A, Leal N, Adasme T, Nunez MT, Hidalgo C. Increased hippocampal expression of the divalent metal transporter 1 (DMT1) mRNA variants 1B and +IRE and DMT1 protein after NMDA-receptor stimulation or spatial memory training. Neurotox Res. 2010; 17:238–247. [PubMed: 19655216]

Holmes-Hampton GP, Chakrabarti M, Cockrell AL, McCormick SP, Abbott LC, Lindahl LS, Lindahl PA. Changing iron content of the mouse brain during development. Metallomics : integrated biometal science. 2012; 4:761–770. [PubMed: 22810488]

Illing AC, Shawki A, Cunningham CL, Mackenzie B. Substrate profile and metal-ion selectivity of human divalent metal-ion transporter-1. J Biol Chem. 2012; 287:30485–30496. [PubMed: 22736759]

Inman RS, Wessling-Resnick M. Characterization of transferrin-independent iron transport in K562 cells. J Biol Chem. 1993; 268:8521–8528. [PubMed: 8473296]

Kaech S, Banker G. Culturing hippocampal neurons. Nat Protoc. 2006; 1:2406–2415. [PubMed: 17406484]

Lambe T, Simpson RJ, Dawson S, et al. Identification of a Steap3 endosomal targeting motif essential for normal iron metabolism. Blood. 2009; 113:1805–1808. [PubMed: 18955558]

Lane DJ, Robinson SR, Czerwinska H, Bishop GM, Lawen A. Two routes of iron accumulation in astrocytes: ascorbate-dependent ferrous iron uptake via the divalent metal transporter (DMT1) plus an independent route for ferric iron. The Biochemical journal. 2010; 432:123–132. [PubMed: 20819077]

Latunde-Dada GO, Simpson RJ, McKie AT. Duodenal cytochrome B expression stimulates iron uptake by human intestinal epithelial cells. Journal of Nutrition. 2008; 138:991–995. [PubMed: 18492824]

Lee DW, Andersen JK. Iron elevations in the aging Parkinsonian brain: a consequence of impaired iron homeostasis? J Neurochem. 2010; 112:332–339. [PubMed: 20085612]

Liu Z, Li H, Soleimani M, Girijashanker K, Reed JM, He L, Dalton TP, Nebert DW. Cd2+ versus Zn2+ uptake by the ZIP8 HCO3--dependent symporter: kinetics, electrogenicity and trafficking. Biochemical and biophysical research communications. 2008; 365:814–820. [PubMed: 18037372]

Liuzzi JP, Aydemir F, Nam H, Knutson MD, Cousins RJ. Zip14 (Slc39a14) mediates non-transferrin-bound iron uptake into cells. Proc Natl Acad Sci USA. 2006; 103:13612–13617. [PubMed: 16950869]

Macia E, Ehrlich M, Massol R, Boucrot E, Brunner C, Kirchhausen T. Dynasore, a cell-permeable inhibitor of dynamin. Dev Cell. 2006; 10:839–850. [PubMed: 16740485]

Mackenzie B, Takanaga H, Hubert N, Rolfs A, Hediger MA. Functional properties of multiple isoforms of human divalent metal-ion transporter 1 (DMT1). The Biochemical journal. 2007; 403:59–69. [PubMed: 17109629]

MacKenzie EL, Iwasaki K, Tsuji Y. Intracellular iron transport and storage: from molecular mechanisms to health implications. Antioxid Redox Signal. 2008; 10:997–1030. [PubMed: 18327971]

McCarthy RC, Kosman DJ. Mechanistic analysis of iron accumulation by endothelial cells of the BBB. Biometals : an international journal on the role of metal ions in biology, biochemistry, and medicine. 2012; 25:665–675.

McCormick SP, Chakrabarti M, Cockrell AL, Park J, Lindahl LS, Lindahl PA. Low-molecular-mass metal complexes in the mouse brain. Metallomics : integrated biometal science. 2013; 5:232–241. [PubMed: 23443205]

McKie AT, Barrow D, Latunde-Dada GO, et al. An iron-regulated ferric reductase associated with the absorption of dietary iron. Science. 2001; 291:1755–1759. [PubMed: 11230685]

Moos T, Morgan EH. Evidence for low molecular weight, non-transferrin-bound iron in rat brain and cerebrospinal fluid. Journal of neuroscience research. 1998; 54:486–494. [PubMed: 9822159]

Moos T, Morgan EH. The metabolism of neuronal iron and its pathogenic role in neurological disease: review. Ann N Y Acad Sci. 2004a; 1012:14–26. [PubMed: 15105252]

Moos T, Morgan EH. The significance of the mutated divalent metal transporter (DMT1) on iron transport into the Belgrade rat brain. Journal of Neurochemistry. 2004b; 88:233–245. [PubMed: 14675167]

Oakhill JS, Marritt SJ, Gareta EG, Cammack R, McKie AT. Functional characterization of human duodenal cytochrome b (Cybrd1): redox properties in relation to iron and ascorbate metabolism. Biochim Biophys Acta. 2008; 1777:260–268. [PubMed: 18194661]

Ohgami RS, Campagna DR, Greer EL, et al. Identification of a ferrireductase required for efficient transferrin-dependent iron uptake in erythroid cells. Nat Genet. 2005; 37:1264–1269. [PubMed: 16227996]

Ohgami RS, Campagna DR, McDonald A, Fleming MD. The Steap proteins are metalloreductases. Blood. 2006; 108:1388–1394. [PubMed: 16609065]

Oshiro S, Nakajima H, Markello T, Krasnewich D, Bernardini I, Gahl WA. Redox, transferrin-independent, and receptor-mediated endocytosis iron uptake systems in cultured human fibroblasts. J Biol Chem. 1993; 268:21586–21591. [PubMed: 8408010]

Pelizzoni I, Macco R, Morini MF, Zacchetti D, Grohovaz F, Codazzi F. Iron handling in hippocampal neurons: activity-dependent iron entry and mitochondria-mediated neurotoxicity. Aging Cell. 2011; 10:172–183. [PubMed: 21108725]

Pelizzoni I, Zacchetti D, Smith CP, Grohovaz F, Codazzi F. Expression of divalent metal transporter 1 in primary hippocampal neurons: reconsidering its role in non-transferrin-bound iron influx. J Neurochem. 2012; 120:269–278. [PubMed: 22121954]

Pinilla-Tenas JJ, Sparkman BK, Shawki A, et al. Zip14 is a complex broad-scope metal-ion transporter whose functional properties support roles in the cellular uptake of zinc and nontransferrin-bound iron. American journal of physiology. Cell physiology. 2011; 301:C862–871. [PubMed: 21653899]

Qian ZM, Ke Y. Brain iron metabolism: neurobiology and neurochemistry. Progress in Neurobiology. 2007; 83:149–173. [PubMed: 17870230]

Salazar J, Mena N, Hunot S, et al. Divalent metal transporter 1 (DMT1) contributes to neurodegeneration in animal models of Parkinson's disease. Proc Natl Acad Sci USA. 2008; 105:18578–18583. [PubMed: 19011085]

Savman K, Nilsson UA, Thoresen M, Kjellmer I. Non-protein-bound iron in brain interstitium of newborn pigs after hypoxia. Developmental neuroscience. 2005; 27:176–184. [PubMed: 16046852]

Siddappa AJ, Rao RB, Wobken JD, Casperson K, Leibold EA, Connor JR, Georgieff MK. Iron deficiency alters iron regulatory protein and iron transport protein expression in the perinatal rat brain. Pediatr Res. 2003; 53:800–807. [PubMed: 12621119]

Siddappa AJ, Rao RB, Wobken JD, Leibold EA, Connor JR, Georgieff MK. Developmental changes in the expression of iron regulatory proteins and iron transport proteins in the perinatal rat brain. Journal of neuroscience research. 2002; 68:761–775. [PubMed: 12111837]

Sturrock A, Alexander J, Lamb J, Craven CM, Kaplan J. Characterization of a transferrin-independent uptake system for iron in HeLa cells. J Biol Chem. 1990; 265:3139–3145. [PubMed: 2105943]

Tabuchi M, Tanaka N, Nishida-Kitayama J, Ohno H, Kishi F. Alternative splicing regulates the subcellular localization of divalent metal transporter 1 isoforms. Mol Biol Cell. 2002; 13:4371–4387. [PubMed: 12475959]

Tabuchi M, Yanatori I, Kawai Y, Kishi F. Retromer-mediated direct sorting is required for proper endosomal recycling of the mammalian iron transporter DMT1. Journal of cell science. 2010; 123:756–766. [PubMed: 20164305]

Thorstensen K. Hepatocytes and reticulocytes have different mechanisms for the uptake of iron from transferrin. J Biol Chem. 1988; 263:16837–16841. [PubMed: 3182815]

Thorstensen K, Romslo I. Uptake of iron from transferrin by isolated rat hepatocytes. A redox-mediated plasma membrane process? J Biol Chem. 1988; 263:8844–8850. [PubMed: 3379048]

Todorich B, Zhang X, Connor JR. H-ferritin is the major source of iron for oligodendrocytes. Glia. 2011; 59:927–935. [PubMed: 21446040]

Tsubaki M, Takeuchi F, Nakanishi N. Cytochrome b561 protein family: expanding roles and versatile transmembrane electron transfer abilities as predicted by a new classification system and protein sequence motif analyses. Biochim Biophys Acta. 2005; 1753:174–190. [PubMed: 16169296]

Tulpule K, Robinson SR, Bishop GM, Dringen R. Uptake of ferrous iron by cultured rat astrocytes. Journal of neuroscience research. 2010; 88:563–571. [PubMed: 19746426]

Vargas JD, Herpers B, McKie AT, Gledhill S, McDonnell J, van den Heuvel M, Davies KE, Ponting CP. Stromal cell-derived receptor 2 and cytochrome b561 are functional ferric reductases. Biochim Biophys Acta. 2003; 1651:116–123. [PubMed: 14499595]

Wang B, Schneider SN, Dragin N, et al. Enhanced cadmium-induced testicular necrosis and renal proximal tubule damage caused by gene-dose increase in a Slc39a8-transgenic mouse line. American journal of physiology. Cell physiology. 2007; 292:C1523–1535. [PubMed: 17108009]

Wang CY, Jenkitkasemwong S, Duarte S, Sparkman B, Shawki A, Mackenzie B, Knutson MD. ZIP8 is an iron and zinc transporter whose cell-surface expression is upregulated by cellular iron loading. J Biol Chem. 2012

Wyman S, Simpson RJ, McKie AT, Sharp PA. Dcytb (Cybrd1) functions as both a ferric and a cupric reductase in vitro. FEBS Lett. 2008; 582:1901–1906. [PubMed: 18498772]

Zecca L, Youdim MB, Riederer P, Connor JR, Crichton RR. Iron, brain ageing and neurodegenerative disorders. Nat Rev Neurosci. 2004; 5:863–873. [PubMed: 15496864]

Zhang DL, Su D, Berczi A, Vargas A, Asard H. An ascorbate-reducible cytochrome b561 is localized in macrophage lysosomes. Biochim Biophys Acta. 2006; 1760:1903–1913. [PubMed: 16996694]

Zhao N, Gao J, Enns CA, Knutson MD. ZRT/IRT-like protein 14 (ZIP14) promotes the cellular assimilation of iron from transferrin. J Biol Chem. 2010; 285:32141–32150. [PubMed: 20682781]

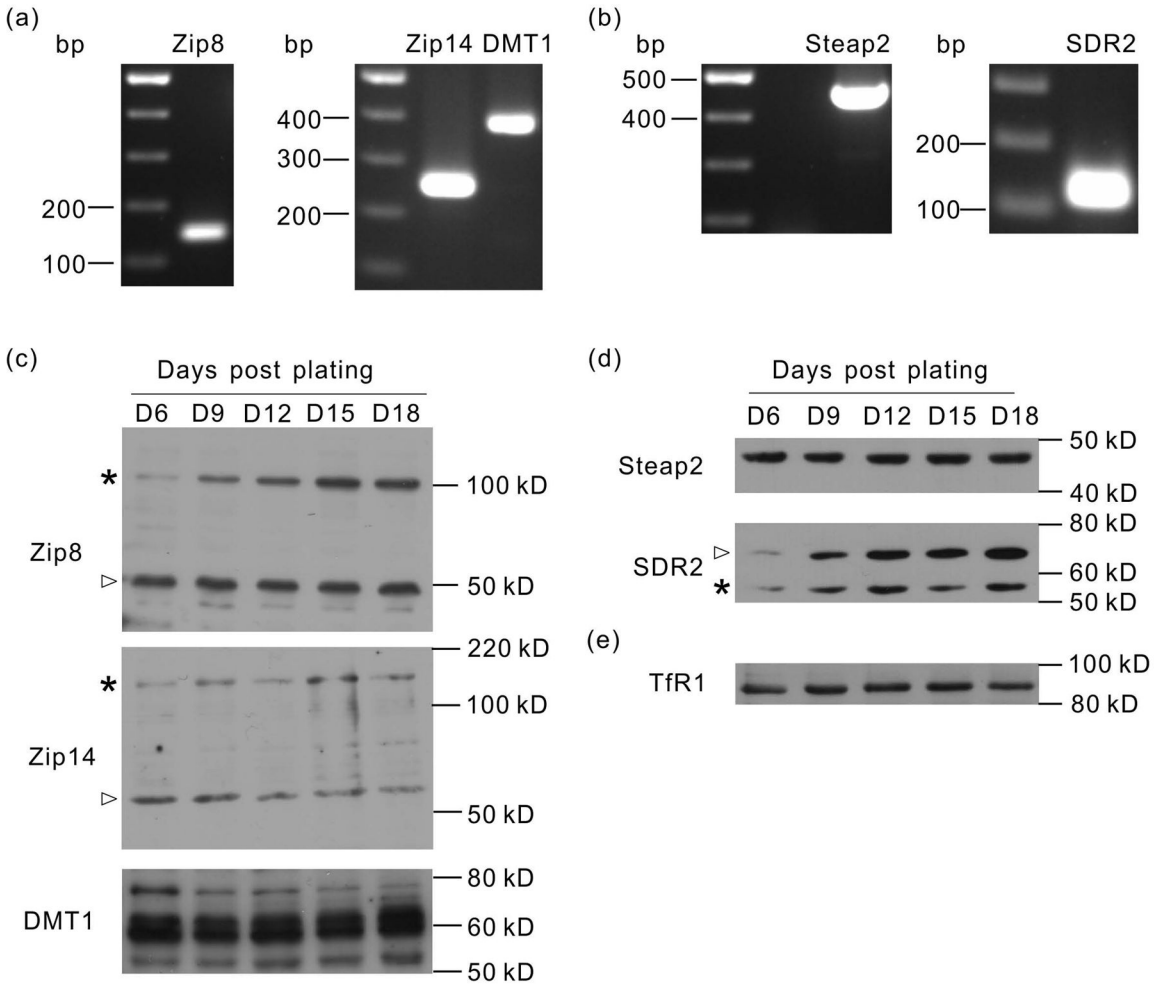


**Fig. 1.**

Expression of iron transport proteins in primary hippocampal neurons. (a) RT-PCR detects the Zip8, Zip14 and 1B-DMT1 transcripts. (b) RT-PCR detects the Steap2 and SDR2 transcripts. (c) Western blot of Zip8, Zip14 and DMT1. Arrowheads highlight species that correlate with the calculated molecular mass of rat Zip8 (NP_001011952.1, ~50 kDa) and Zip14 (NP_001100745.1, ~54 kDa). In the Zip8 immunoblots, a higher molecular mass species (100 kDa, *) was detected and likely represents the Zip8 dimer. In Zip14 immunoblots, a higher molecular mass species (150 kDa, *) was detected and may represent a glycosylated form of Zip14. In DMT1 immunoblots, several bands near the predicted molecular mass of DMT1 (~62 – 64 kDa) were observed which likely represent the different isoforms of DMT1 expressed in these cells. (d) Western blot of Steap2 and SDR2. In SDR2 immunoblots, the arrowhead indicates the band that correlate with the calculated molecular mass of rat SDR2 (XP_008773478.1, ~66 kDa); the lower band (*) may represent a degraded form of SDR2 associated with the acetone precipitation method used to prepare a concentrated protein lysate. (e) TfR expression in primary hippocampal neurons. In c-e, neuronal lysates were collected as a function of days post plating.

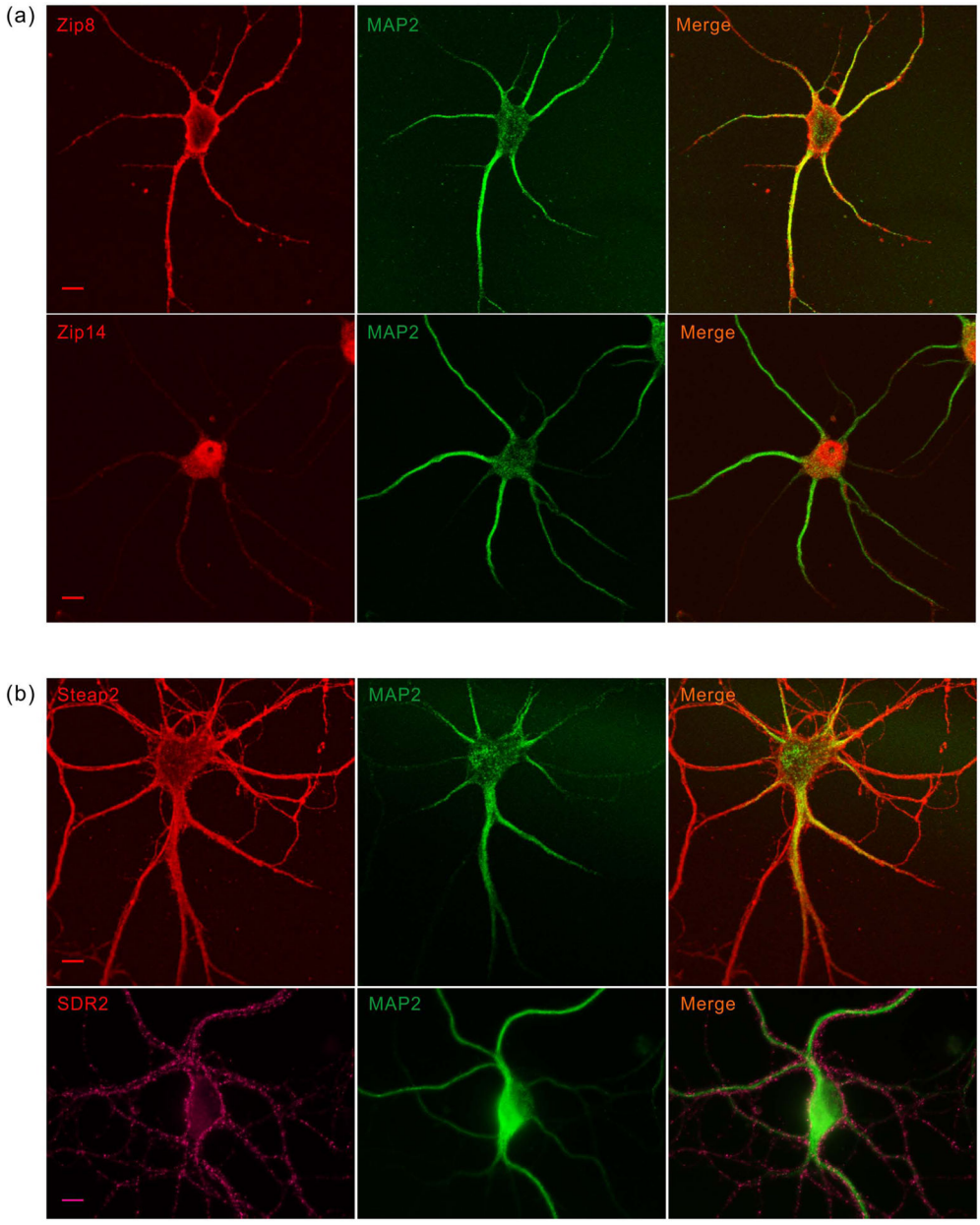


**Fig. 2.**

Localization of Zip8, Zip14, Steap2 and SDR2 in primary hippocampal neurons. (a) Confocal images indicate Zip8 predominates on the cell surface, while Zip14 has an intracellular localization. (b) Confocal images of Steap2 and SDR2 indicate that Steap2 has both cell surface and intracellular localization, while SDR2 is visualized only on the cell surface. MAP2 is a neuron-specific marker. The images are representative of 5 cells examined in each of three independent experiments. Scale bar: 10 μm.

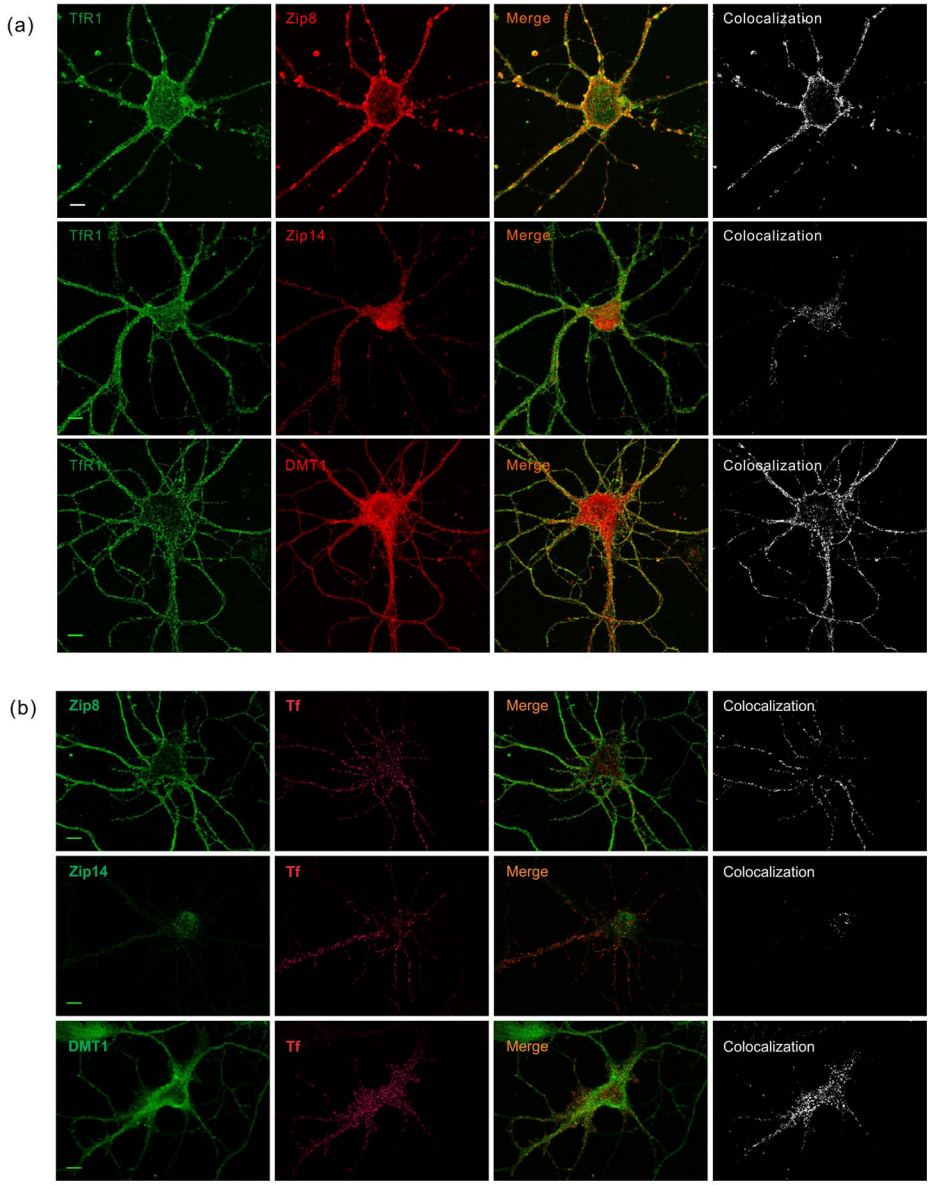


**Fig. 3.**

Co-localization of ferrous iron transporters with TfR or Tf-594. (a) Confocal analysis of endogenous Zip8, Zip14 or DMT1 with TfR. Zip8 immunofluorescence signal has a strong overlap with TfR on the cell surface of both neuronal soma and processes. Zip14 shows intracellular co-localization with TfR primarily on the cell body. DMT1 and TfR partially co-localize with each other on both soma and processes. (b) Immunofluorescence analysis of Zip8, Zip14 or DMT1 with Alexa Fluor 594 conjugated Tf (Tf-594). Tf-594 (50 μM) was incubated with primary hippocampal neurons at 37°C for 5 min, then excess Tf-594 removed by washing. Cells were fixed and immunostained with anti-Zip8, anti-Zip14 or anti-DMT1. Zip8 staining overlaps the Tf-594 fluorescence signal associated with neuronal processes. Zip14 signal does not co-localize with Tf-594. DMT1 co-localizes with Tf-594 in

the soma. The images are representative of 5 cells examined in two independent experiments. Scale bar: 10 μm.

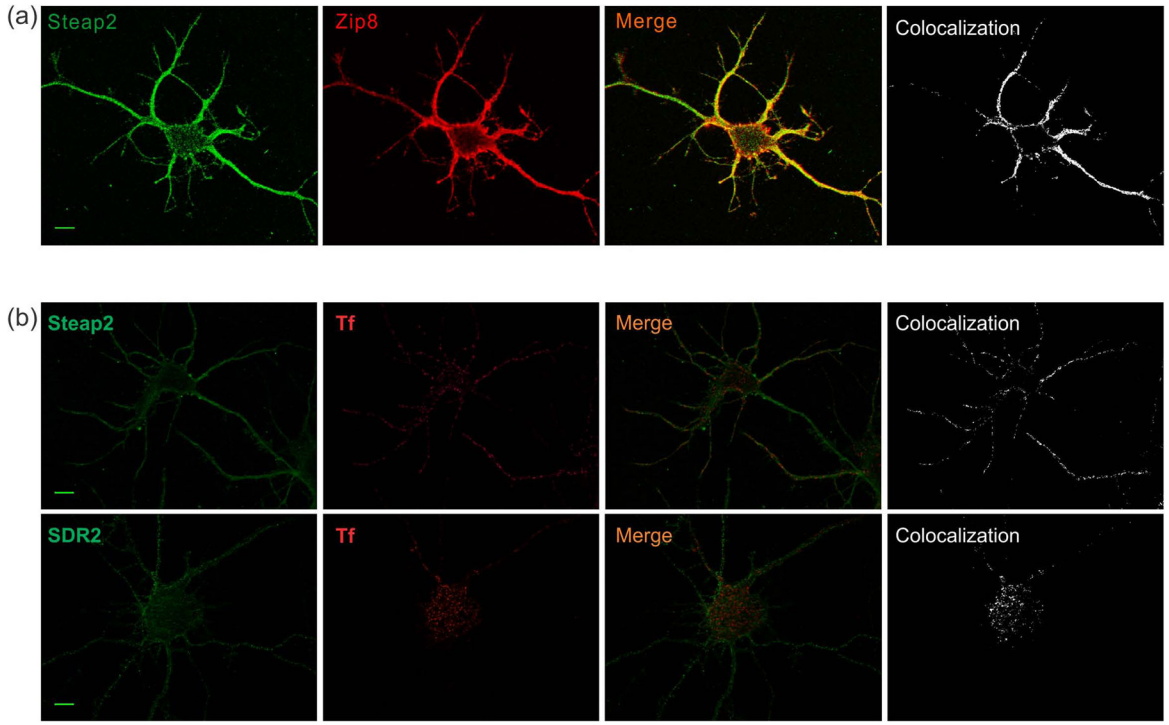


**Fig. 4.**

Co-localization of ferrireductase and iron transport proteins. (a) Confocal analysis of endogenous Steap2 and Zip8 indicates that Steap2 co-localizes with Zip8 on the cell surface of neuronal soma and processes. (b) Immunofluorescence analysis of Steap2 or SDR2 with Tf-594 [method as in Fig. 3(b)]. Steap2 is partially co-localized with Tf-594 at the neuronal soma and processes. SDR2 immunofluorescence partially overlapped with Tf-594 in the neuronal soma. The images are representative of 5 cells in examined in two independent experiments. Scale bar: 10 μm.

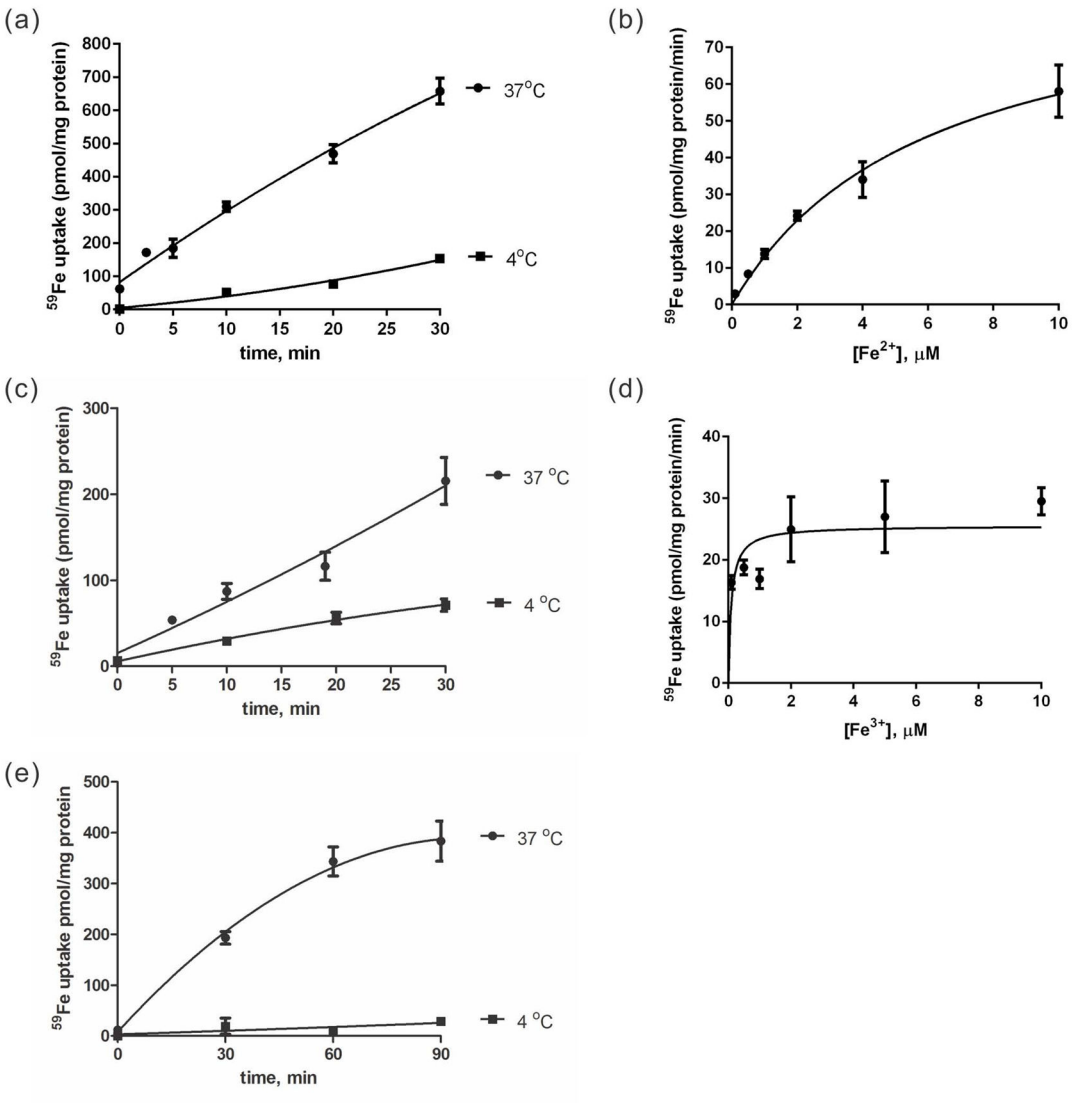


**Fig. 5.**

$^{59}Fe$ uptake from NTBI and TBI is active in primary hippocampal neurons. (a) $^{59}Fe^{2+}$ uptake is time and temperature-dependent. $^{59}Fe^{2+}$ (1 μM as the citrate complex) was incubated with neurons at 37 °C or 4 °C. (b) $Fe^{2+}$ uptake is concentration-dependent. Initial velocity of $Fe^{2+}$ uptake was calculated from the rate of $^{59}Fe^{2+}$ accumulation in first 10 minutes; the Michaelis-Menten equation was used to fit the data ($r^2 = 0.9662$). (c) $^{59}Fe^{3+}$ uptake is time-dependent and temperature-dependent in primary hippocampal neurons. $^{59}Fe^{3+}$-citrate (1 μM) was incubated with neurons at 37°C or 4°C. (d) $Fe^{3+}$ uptake is concentration-dependent (method as directly above). Note that the lack of velocity data at [Fe] < $K_M$ strongly limits the significance of this fit ($r^2 = 0.3661$). (e) Time course of $^{59}Fe$ uptake from $^{59}Fe$-transferrin ($^{59}Fe$-Tf). $^{59}Fe$-Tf (0.5 μM Tf, 1.0 μM $^{59}Fe$) was incubated with neurons at 37°C or 4°C. All experiments were performed twice; in each experiment, 4 technical replicates were taken at each experimental point.

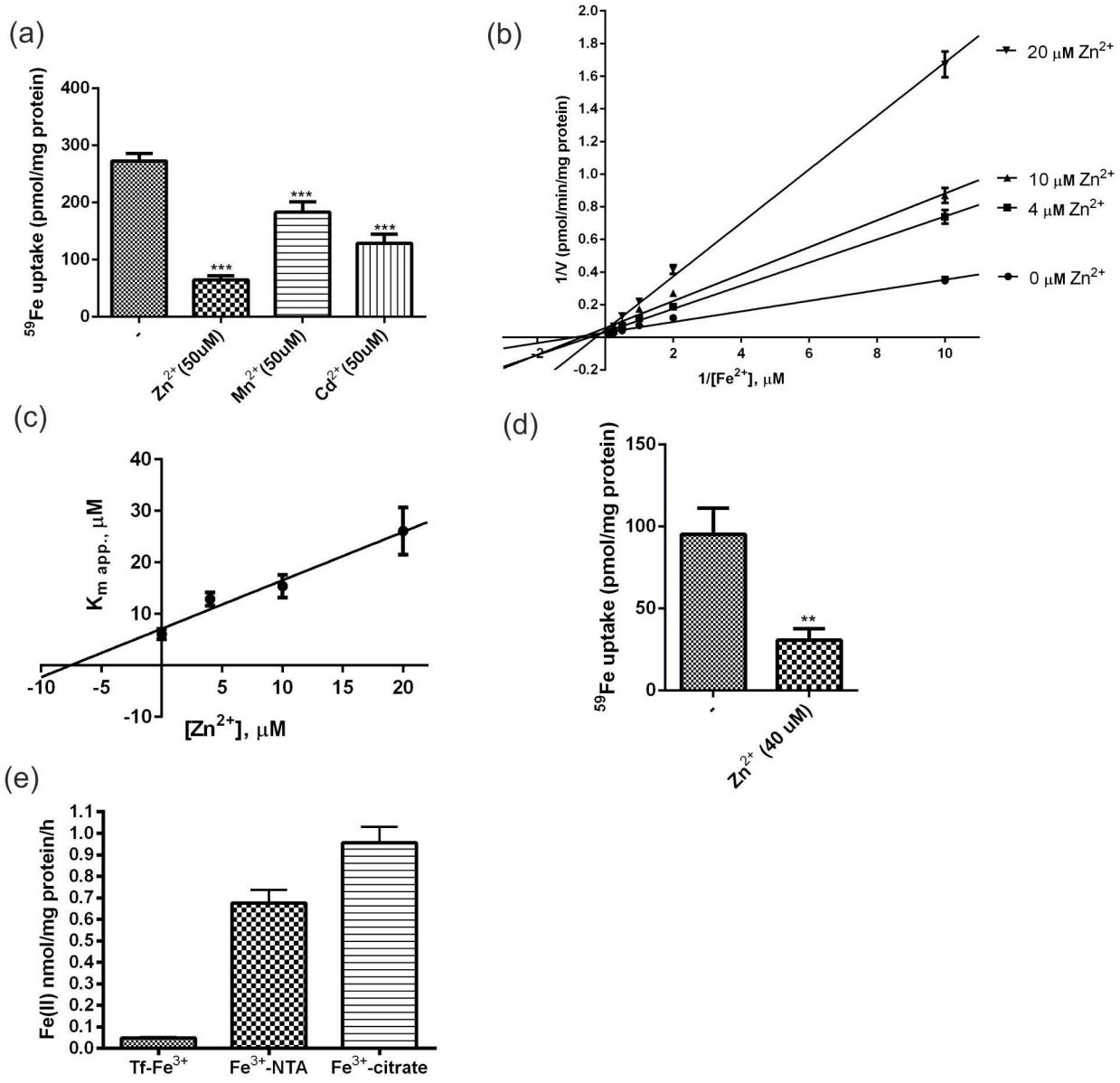


**Fig. 6.**

$^{59}Fe$ uptake from NTBI is inhibited by divalent metal ions in primary hippocampal neurons. (a) $Fe^{2+}$ uptake is inhibited by $Zn^{2+}$, $Mn^{2+}$ and $Cd^{2+}$. $^{59}Fe^{2+}$-citrate (1 μM) was added along with 50 μM $Zn^{2+}$, $Mn^{2+}$ or $Cd^{2+}$. Experiments were performed twice; in each experiment, 3 replicates were observed in each condition. Statistical significance was tested by one-way ANOVA followed by Bonferroni pair-wise comparison *post hoc* tests. ***, $p < 0.001$. None of the metal ion competitors exhibited cytotoxicity at the concentrations employed (Fig. S1). (b) Kinetic analyses of $Zn^{2+}$ inhibition of $^{59}Fe^{2+}$ uptake. $^{59}Fe^{2+}$ uptake rates were determined in the presence of different $Zn^{2+}$ concentrations; the data are presented in reciprocal form based on fitting the Michaelis-Menten equation to each data set. Data are from one experiment with 4 technical replicates for each data point. (c) A linear regression analysis of the $K_m$(app) values derived from the data shown in 6(b) ($r^2 = 0.9690$). This replot

provided a $K_i$ value for $Zn^{2+}$, 7.6 μM. (d) $^{59}Fe^{3+}$ uptake was inhibited by $Zn^{2+}$. $^{59}Fe^{3+}$-citrate (1 μM) was incubated with neurons in the absence or presence of 40 μM $Zn^{2+}$. Data are from two separate experiments with 4 technical replicates for each data point. Significance was tested by the unpaired t test: **, $p < 0.01$. (e) Primary hippocampal neurons exhibit ferrireductase activity when incubated with ferric iron substrates: TBI (Tf-$Fe^{3+}$), or NTBI ($Fe^{3+}$-NTA, $Fe^{3+}$-Citrate). Data are from two separate experiments with 3 technical replicates for each data point.

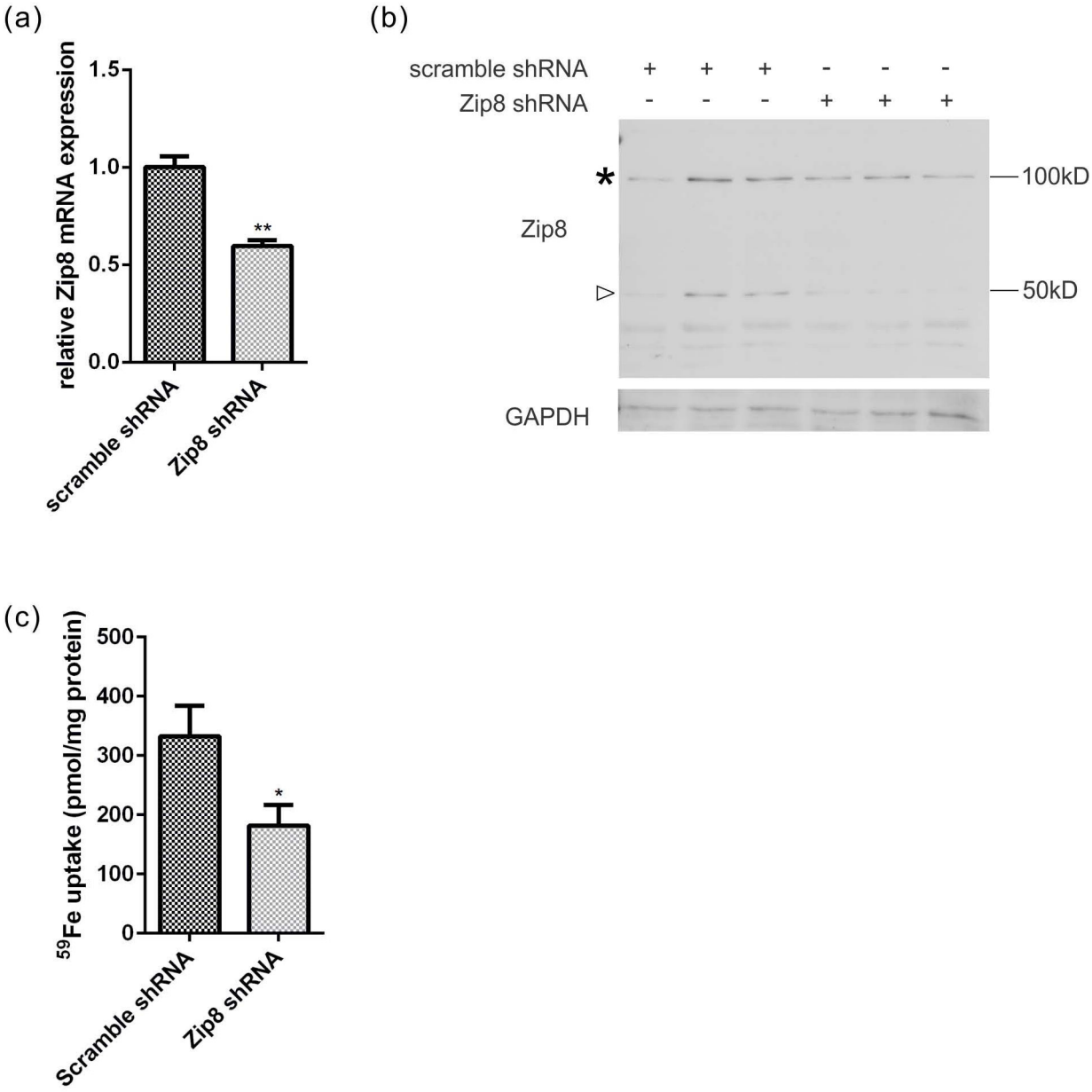


**Fig. 7.**

Zip8 knockdown results in a decrease of $Fe^{2+}$ uptake in primary hippocampal neurons. (a) Zip8 transcript is decreased in Zip8 shRNA knockdown. (b) Zip8 expression is reduced at the protein level in neurons with Zip8 shRNA knockdown. Decreases of Zip8 expression were observed with respect to both 50 kDa (arrowhead) and 100 kDa (*) bands. (c) $Fe^{2+}$ uptake is decreased in Zip8 knockdown neurons. $^{59}Fe^{2+}$-citrate (1 μM) was incubated with neurons at 37°C for 30 min. Data are from one experiment with 5 technical replicates for each data point. Statistical significance was tested by the unpaired t test. *, $p < 0.05$, ** $p < 0.01$.

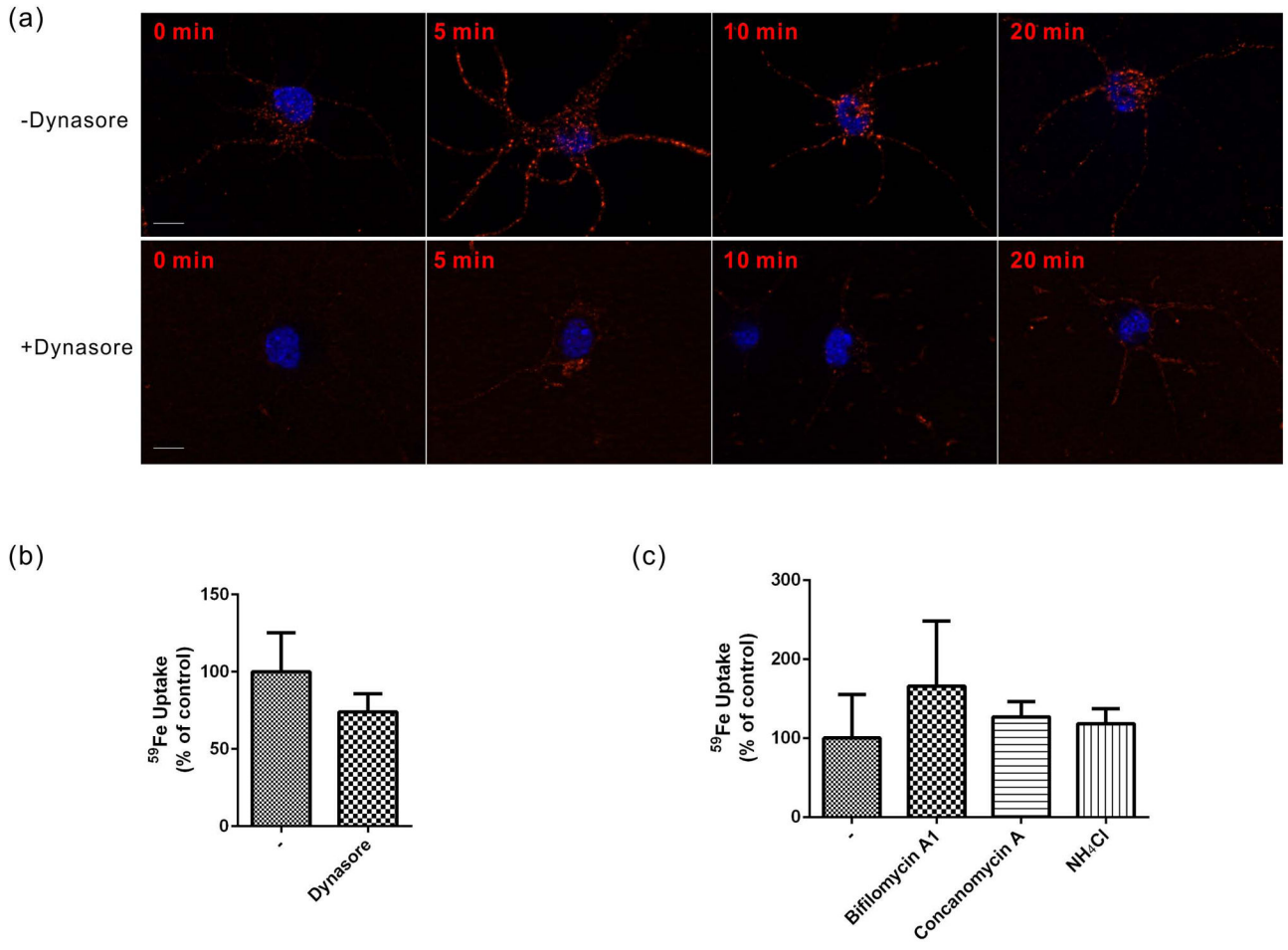


**Fig. 8.**

TBI uptake is not sensitive to the inhibition of endocytosis or endosomal acidification in primary hippocampal neurons. (a) Dynasore inhibits Tf-594 internalization. Neurons are pre-incubated in the absence or presence of 80 μM dynasore for 30 min at room temperature followed by incubation with 50 μM Tf-594 for 2 min. After a brief wash with Tf-free buffer, the cultures were returned to 37°C and incubated for the time period indicated. DAPI stains the nuclei. The images are representative of 5 cells in two independent experiments. Scale bar: 10 μm. (b) Dynasore does not significantly inhibit $^{59}$Fe-Tf iron uptake. Neurons were pre-incubated in the absence or presence of 80 μM dynasore for 30 min, followed by incubation with $^{59}$Fe-Tf (0.5 μM Tf, 1.0 μM $^{59}$Fe) at 37°C for 1 hour. Experiments were performed twice; 4 replicates were observed in each condition. Significance was tested by the unpaired t test, n.s. (c) Neither inhibition of $H^+$-ATPase (Bifilomycin A1 or Concanamycin A), nor ablation of endosomal acidification ($NH_4Cl$) significantly affects Fe uptake from $^{59}$Fe-Tf. Neurons were pretreated with 500 nM Bifilomycin A1, or 50 nM Concanamycin A, or 10 mM $NH_4Cl$ for 30 min, followed by incubation with $^{59}$Fe-Tf (0.5 μM Tf, 1.0 μM $^{59}$Fe) at 37°C for 1 h. Data are from two experiments with 5 technical replicates for each data point. Significance was tested by one-way ANOVA, n.s.